8-2014

100 kHz, 100 ms, 400 J burst-mode laser with dual-wavelength diode-pumped amplifiers

Mikhail N. Slipchenko
Spectral Energies

Joseph D. Miller
Air Force Research Laboratory

Sukesh Roy
Spectral Energies

Terrence R. Meyer
Iowa State University, trm@iastate.edu

Jason G. Mance
Spectral Energies

See next page for additional authors

100 kHz, 100 ms, 400 J burst-mode laser with dual-wavelength diode-pumped amplifiers

Abstract
The burst duration of an all-diode-pumped burst-mode laser is extended to 100 ms and 100 kHz (10,000 pulses) by utilizing dual-wavelength diode pumping. Total energies of 225 J at 10 kHz and 400 J at 100 kHz are achieved during the 100 ms burst period at 1064 nm. This represents an order-of-magnitude increase in the number of pulses compared with prior work, while maintaining similar or higher pulse energies. Amplitude tailoring of each pulse is used to flatten the burst profile, reducing the standard deviation in pulse energy over the 100 ms burst from 3.7% to 2.1% with a burst-to-burst standard deviation of 0.8%.

Keywords
statistics, diodes, optical pumping, burst period, diode-pumped, pulse energies, standard deviation, total energy, dual wavelength

Disciplines
Mechanical Engineering | Statistics and Probability

Comments
This article is from *Optics Letters* 39 (2014): 4735, doi: 10.1364/OL.39.004735. Posted with permission.

Authors
Mikhail N. Slipchenko, Joseph D. Miller, Sukesh Roy, Terrence R. Meyer, Jason G. Mance, and James R. Gord

100 kHz, 100 ms, 400 J burst-mode laser with dual-wavelength diode-pumped amplifiers

Mikhail N. Slipchenko,[1] Joseph D. Miller,[2] Sukesh Roy,[1] Terrence R. Meyer,[3] Jason G. Mance,[1] and James R. Gord[2,*]

[1]*Spectral Energies, LLC, Dayton, Ohio 45431, USA*

[2]*Air Force Research Laboratory, Aerospace Systems Directorate, Wright-Patterson AFB, Ohio 45433, USA*

[3]*Department of Mechanical Engineering, Iowa State University, Ames, Iowa 50011, USA*

**Corresponding author: james.gord@us.af.mil*

Received May 22, 2014; revised July 1, 2014; accepted July 2, 2014;
posted July 9, 2014 (Doc. ID 212583); published August 7, 2014

The burst duration of an all-diode-pumped burst-mode laser is extended to 100 ms and 100 kHz (10,000 pulses) by utilizing dual-wavelength diode pumping. Total energies of 225 J at 10 kHz and 400 J at 100 kHz are achieved during the 100 ms burst period at 1064 nm. This represents an order-of-magnitude increase in the number of pulses compared with prior work, while maintaining similar or higher pulse energies. Amplitude tailoring of each pulse is used to flatten the burst profile, reducing the standard deviation in pulse energy over the 100 ms burst from 3.7% to 2.1% with a burst-to-burst standard deviation of 0.8%. © 2014 Optical Society of America

OCIS codes: (120.1740) Combustion diagnostics; (140.3280) Laser amplifiers; (140.3480) Lasers, diode-pumped; (140.3538) Lasers, pulsed.

http://dx.doi.org/10.1364/OL.39.004735

Laser-based measurements with high temporal and spatial resolution of transient processes in turbulent combustion require significant pulse energies at repetition rates exceeding 1 kHz. Continuously pulsed diode-pumped solid-state (DPSS) lasers used for this purpose [1,2] have improved significantly and can now produce average powers of 600 W at 1064 nm and 200 W at 532 nm for repetition rates up to 150 kHz [3]. At 1064 nm, for example, this corresponds to 60 mJ per pulse at 10 kHz and 6 mJ per pulse at 100 kHz.

To overcome limitations on laser energy and improve signal-to-noise ratio (SNR) further, it is necessary to consider the use of burst-mode laser technology. Burst-mode lasers achieve high pulse energy (hundreds of mJs for ns pulse durations and several mJs for subpicosecond pulse durations) in combination with high-repetition-rate operation (10–1000 kHz) by grouping a series of 100 or more closely spaced pulses into short bursts, thus enabling high pulse peak power with low average system power [4,5]. The main disadvantage of burst-mode operation relative to continuously pulsed sources is the limited number of pulses, limited burst duration, or both. Initial work with flashlamp-pumped, Nd:YAG-based burst-mode systems was limited by the flashlamp drivers to only a few pulses for a duration of ~200 μs [6]. As such, early work focused on 1 MHz flow visualization in supersonic flows [6,7]. Multichannel Nd:YAG lasers allow greater flexibility and higher pulse energy by utilizing independent laser oscillators, but are not readily scalable beyond eight pulses. However, these have been used for high-speed planar Raman measurements at 10 kHz, but only for time periods of 0.7 ms [8]. Continuing work on burst-mode operation improved pulse sequences to ~1–2 ms at 25–50 kHz with up to 28 pulses (limited by the camera) by utilizing extended-duration flashlamp drivers [9], and then to 10 ms by utilizing a combination of flashlamp and diode-pumped stages [10]. The longest burst duration of 30 ms at 5 kHz was then achieved by Slipchenko *et al.* [11], relying exclusively on diode-pumped amplification stages. That system was used for planar laser-induced fluorescence (PLIF) measurements of formaldehyde in lifted jet diffusion flames. In addition to extended burst duration, diode-pumped amplifiers offered higher electrical-to-optical efficiency among other advantages. Meanwhile, the ability to extend the duration of flashlamp pulses enabled bursts up to 13 ms at 10 kHz [12] and up to 10 ms at 100 kHz [13]. The latter again utilized a combination of flashlamp and diode-pumped stages, and represented the largest number of pulses achieved with a burst-mode laser system for combustion diagnostics.

While these represent significant improvements in burst-mode laser technology, extending the duration of pulse sequences beyond 30 ms for repetition rates higher than 5 kHz was found to be limited by temperature-dependent shifting of the diode wavelengths used for amplification. As such, previous work [11] reported significant variation in the pulse energy during the burst, requiring corrections for laser intensity variations and potentially reducing the SNR later in the pulse sequence. In this Letter, we report on an all-diode-pumped quasi-continuous burst-mode (QCBM) laser system with dual-wavelength pumping, which mitigates the wavelength-shift limitation of the previous design. This allows extension of the pulse sequence from 30 to 100 ms, an increase in the repetition rate from 5 to 100 kHz during this longer time period and a significant improvement in the uniformity of the pulse energy throughout the burst. The average pulse energy is 225 mJ at 10 kHz (1000 pulses) and 40 mJ at 100 kHz (10,000 pulses). This performance represents a ~10× increase in reported burst duration and number of pulses at 10–100 kHz compared to current flashlamp-based systems [10,12,13].

The all-diode-pumped dual-wavelength QCBM laser architecture is similar to our previous system [11], which utilizes a master oscillator power amplifier design for amplifying a burst of high-repetition-rate pulses through Nd:YAG-based amplifiers, as shown in Fig. 1. A 130 mW

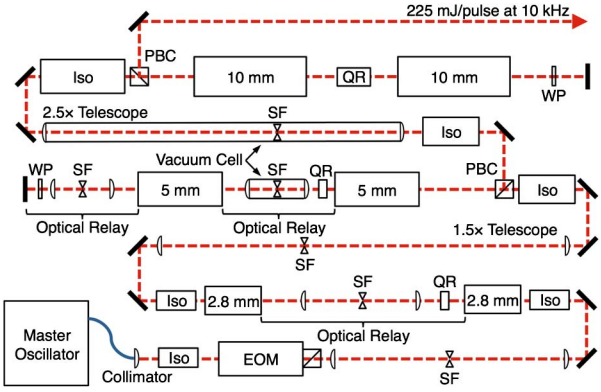

Fig. 1. Schematic of 100 ms, all-diode-pumped burst-mode laser system. Dashed line represents beam pathway through system. Diode amplifiers are listed by rod diameter. Iso, optical isolator; EOM, electro-optic modulator; SF, spatial filter; QR, quartz rotator; PBC, polarizing beam cube; WP, quarter-wave plate.

continuous-wave (CW) fiber-coupled diode laser at 1064.339 nm (vac) with bandwidth of 280 MHz is sliced into individual pulses at 10–100 kHz using a fiber-coupled acousto-optic modulator (AOM) with a 10 ns rise/fall time. Pulse width and amplitude can be independently adjusted via the analog modulation input of the AOM. The pulsed output is preamplified to 2 μJ at 10 kHz and 0.65 μJ at 100 kHz in a multistage fiber amplifier. Large-mode-area polarization-maintaining fiber is used to ensure high beam quality (Gaussian $M^2 = 1.15$) entering the free-space power amplifiers. To reduce CW background, the burst is gated by an electro-optic modulator (EOM) located directly before the first amplifier stage. The EOM voltage (and, therefore, pulse intensity, burst duration, and burst shape) is modulated using an arbitrary waveform generator with either a DC offset or user-defined waveform. The overall extinction ratio of the AOM/EOM combination is greater than 60 dB.

The power amplifier consists of three pairs of diode-pumped Nd:YAG amplifiers (0.6% Nd doping) with rod diameters of 2.8, 5, and 10 mm. Two 2.8 mm amplifier stages are operated in a single-pass configuration, while two 5 mm and two 10 mm stages are operated in double-pass configurations, as shown in Fig. 1. Optical relays are used between each 2.8 and 5 mm amplifier, and also between each pair. The beam diameter is increased ~1.5× between the 2.8 and 5 mm stages and ~2.5× between the 5 and 10 mm stages, resulting in an output beam diameter of 7.3 mm. To minimize the amplified spontaneous emission (ASE) and improve beam quality, pinholes are placed at the focal points of the optical relays. Together with the high extinction ratio of the AOM/EOM combination, these strategies allow minimization of ASE output (<10%). Note while the use of a stimulated-Brillouin-scattering phase-conjugate mirror (SBS-PCM) completely removes ASE, the nonlinearity of the SBS effect severely limits the adjustment of pulse repetition rate, can increase pulse-to-pulse instabilities, and can result in pulse width variation as a function of burst duration [12]. On the contrary, AOM/EOM gating allows straightforward adjustment of pulse repetition rate without degradation of the energy extraction efficiency or pulse-to-pulse stability. Each burst is separated by 8 s to allow thermal relaxation of the amplifier stages.

The primary innovations in this work are extension of diode-pumped amplifier operation beyond 30 ms and significant increase in burst uniformity for higher repetition rates using dual-wavelength pumping. In typical single-wavelength diode-pumped Nd:YAG amplifiers [10,11], the diode-array output is centered at 808 nm with a bandwidth of ~2 nm for optimal overlap with the $^4I_{9/2} \rightarrow {}^4F_{5/2}$ transition, as shown in Fig. 2(a) [14]. Under quasi-continuous operation, the temperature of the diode arrays changes with time because of resistance heating (electrical-to-optical efficiency of the diodes is ~50%). As a result, the diode wavelengths shift toward higher wavelengths with increased temperature (~0.25 nm/°C). As the central wavelength passes the $^4I_{9/2} \rightarrow {}^4F_{5/2}$ absorption peak, the small-signal gain profile rises and falls, as shown in Fig. 2(b) for a 5 mm amplifier with single-wavelength arrays (SWAs). The small-signal gain reaches 25× at 10 ms, but falls to 7× at 40 ms. Such a large change in small-signal gain produces considerable drop in the output pulse energy beyond 30 ms; therefore, nearly uniform gain profiles are necessary for extended duration amplification [11].

To extend the pump duration to 100 ms, the limitation of the SWA amplifier is overcome by utilizing custom diode-pumped Nd:YAG amplifiers with diode arrays operating at two separate center wavelengths. The center wavelengths are selected to be 2.7 nm higher and 3.3 nm lower than that of the SWA, and are shown relative to the maximum Nd:YAG absorption in Fig. 2(a) [15]. To incorporate this design, the total number of arrays per amplifier (40 arrays per 2.8 mm amplifier, 80 arrays per 5 mm amplifier, and 140 arrays per 10 mm amplifier) is split evenly between the two wavelengths, thus

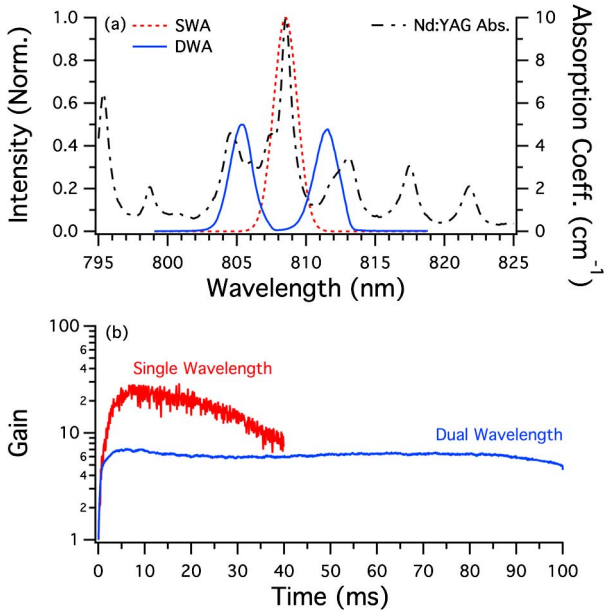

Fig. 2. (a) Comparison of single-wavelength array (SWA) and dual-wavelength array (DWA) diode emission relative to 808 nm Nd:YAG absorption [15], and (b) time-dependent small-signal gain of 5 mm SWA and DWA amplifiers.

maintaining the same total power as the SWA but with lower spectral power density. Note that the laser output wavelength does not depend on the diode-bar wavelength, which only influences the absorption, and therefore gain, of the amplifiers.

The effect of the dual-wavelength arrays (DWAs) on the small-signal gain is evident from the nearly uniform profile in Fig. 2(b). The average gain (6.5×) is lower because of the wavelength splitting; however, the pump duration is increased more than twofold, allowing operation up to 100 ms. In the current work, all six diode amplifiers are DWA configured, allowing operation of the entire system with bursts as long as 100 ms. Under normal long-burst operating conditions, the small-signal, single-pass gain of the 2.8, 5, and 10 mm stages are 1.5, 6.5, and 9, respectively.

The measured gain of the system, including the fiber-amplifier-enhanced oscillator and free-space power amplifiers, is $\sim 3.9 \times 10^8$ at 10 kHz, and the average pulse energy over the 100 ms burst is given as a function of electrical energy delivered to the diodes for 10, 25, 50, and 100 kHz in Fig. 3(a). The stored energy in each amplifier can be estimated assuming 50% electrical-to-optical efficiency and 42% absorption [15]. At electrical energy greater than 4.5 kJ, the system operates in a nearly saturated manner, where the individual pulse energies increase linearly with stored energy in the amplifiers. The maximum output energy is given explicitly as a function of repetition rate in Fig. 3(b), fit using power law scaling ($ax^b + c$ where $a = 752.17$, $b = -0.3093$, and $c = -143.89$), and compared with the theoretical pulse energy of a 600 W DPSS laser. DPSS lasers for material processing can reach even higher average powers of 1.6 kW at 1064 nm [16] and 420 W at 532 nm [17], but at the expense of long pulse durations, up to 100 ns, and M^2 factor of ~30. The individual pulse energy was calculated from the total burst energy measured using a thermal power meter (Ophir FL250A-RP) by subtracting the ASE contribution and dividing by the total number of pulses. The ASE contribution was measured by blocking the master oscillator. The ~10% ASE contribution should be taken as an upper-limit measurement since the stored energy was not removed via pulses during the measurement, thus maximizing ASE gain. The pulse energy of 139 mJ per pulse at 25 kHz and 100 ms (2500 pulses) is similar to that achieved in previous work at a lower repetition rate of 10 kHz and shorter duration of 10 ms (100 pulses) [10]. Additionally, the fundamental energy of 40 mJ available at 100 kHz and 100 ms (10,000 pulses) is similar to that used for CH_2O PLIF at 100 kHz and 10 ms (1000 pulses) [13], providing a tenfold increase in burst duration and number of pulses without a significant reduction in pulse energy.

A typical 100 ms burst is shown in Fig. 4(a) (upper red line), where each point represents the energy of an individual 10 ns pulse at 10 kHz, as shown in Figs. 4(b) and 4(c). The burst profile was recorded with a biased silicon photodiode with 1 ns rise time and ground glass diffuser (Thorlabs DET10A). Because no change in pulse width is observed as a function of burst duration, the pulse energy can be directly related to peak photodiode voltage, allowing the calculation of individual pulse energies via a scaling factor determined as a function of burst energy divided by pulse number weighted by peak intensity.

The variation of pulse energy with time originates from the modulation of the oscillator pulse train (standard deviation of ~1%) with the gain profiles of each amplifier. The peak-to-peak variation of 16.4% in the upper unshaped profile in Fig. 4(a) is slightly smaller than that of the small-signal gain profile of the 5 mm amplifier,

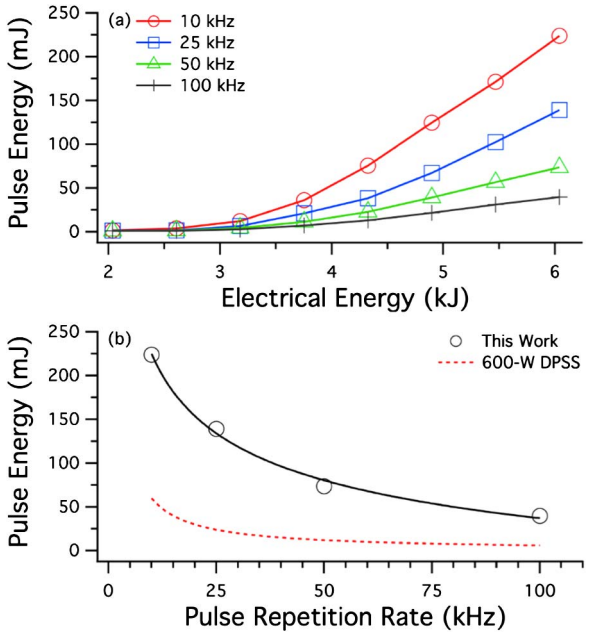

Fig. 3. Individual pulse energy as a function of (a) total electrical energy delivered to the system and (b) pulse repetition rate. Burst-to-burst standard deviation of 0.8% falls within the symbol size. The experimental data is fit to a power law scaling and compared with the calculated performance of a 600 W DPSS laser [3].

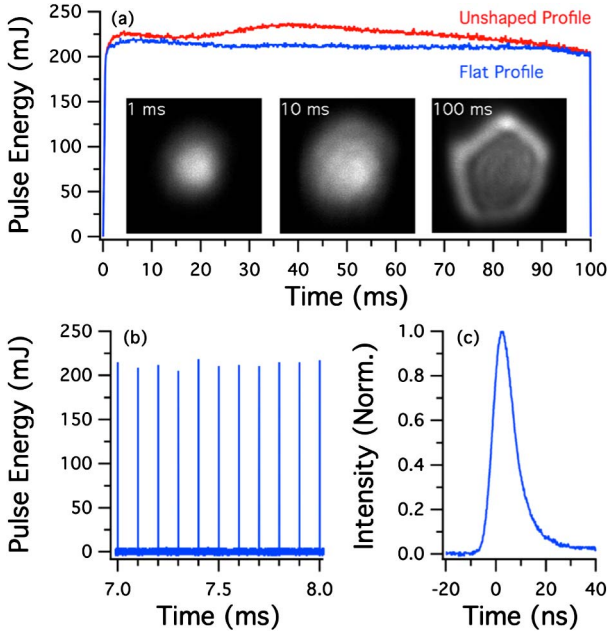

Fig. 4. (a) Comparison of unshaped and flat-top burst-profile pulse energies over 100 ms. (b) 1 ms segment of (a) showing 10 kHz operation, and (c) profile of an individual pulse with pulse width of 9.85 ns (FWHM).

22.6%. This reduction results primarily from operating the 10 mm amplifiers in a nearly saturated manner [at electrical energies >4.5 kJ, as shown in Fig. 3(a)]. The standard deviation of the unshaped burst profile is 3.7% (8.3 mJ) with mean pulse energy of 225 mJ over the entire 100 ms burst. This represents a significant improvement of the burst uniformity compared to the 5 kHz, 30 ms pulse sequence reported in prior work using a single-wavelength, all-diode-pumped design [11]. As with this previous work, the burst-to-burst repeatability of the burst profile and total energy is excellent, with a standard deviation of 0.8%.

Even so, there are many applications where it is critical either to reduce peak-to-peak energy variations within the burst in order to optimize measurement detection efficiency and sensitivity, or to shape the burst profile to control energy delivery to a probe volume. For this purpose, we have incorporated an arbitrary waveform generator to provide single-pulse shaping of the burst by controlling the input pulse energy into the power amplifier stages. By measuring the modulation transfer through all six amplifier stages, we can reliably reproduce the system performance for controlling the output energy of each pulse. This is performed by modulating transmission through the EOM via the set voltage, resulting in pulse intensity reduction up to 20×. The corresponding output intensity, however, can only be reduced 2.5× due to the large system gain. The time-dependent correction waveform is generated by comparing the natural profile shape with the desired profile and then multiplying the difference by the modulation transfer through the power amplifiers. For improved accuracy, several iterations of this process can be performed to converge on the desired profile.

A typical tailored burst with flat-top profile is shown alongside the unshaped profile in Fig. 4(a) (bottom blue line). While the average pulse energy is reduced by 5.8% to 212 mJ, shaping the burst produces a nearly twofold reduction in peak-to-peak energy variation of 9.9% and standard deviation of 2.1% (4.5 mJ), providing a flat burst profile (99.97% flatness as defined by the ratio of the geometric to arithmetic means). As a point of comparison, these values measured over 100 ms are less than a third of the RMS value (7%–9%) and half of the peak-to-peak value (~20%) reported for similar flashlamp-pumped systems over only 13 ms [12]. Additionally, the ability to generate arbitrary burst profiles could be used for time-varying energy delivery or matched-filtering applications.

As was discussed in our previous work [11], the beam profile changes during the burst due to the buildup of thermal gradients in the Nd:YAG rods [as shown in Fig. 4(a)] at 1, 10, and 100 ms. The beam profile has a nearly Gaussian shape for the first 20 ms, after which the thermal lensing results in nonoptimal passage through the pinholes and amplifiers. As a result, interference rings appear in the output beam, particularly after 70 ms, creating a flat-top and eventually ring-like profile.

In summary, up to 1000 pulses with 225 mJ per pulse at 1064 nm were generated at 10 kHz repetition rate (225 J per burst), and up to 10,000 pulses with 40 mJ per pulse at 1064 nm were generated at 100 kHz repetition rate (400 J per burst) using a dual-wavelength, all-diode-pumped burst-mode laser. This is a tenfold increase in the number of pulses and burst duration at 10–100 kHz. This laser architecture also achieves excellent uniformity in pulse energy throughout the burst, representing an improvement over previous designs operating at only 10 ms. Furthermore, shaping of the burst profile via EOM transmission modulation yields a significant decrease in peak-to-peak energy variation (from 16.5% to 9.9%) and standard deviation (from 3.7% to 2.1%), with only a 5.8% decrease in average pulse energy (212 mJ at 10 kHz). This system shows great promise as a robust source for high-speed multiparameter measurements in turbulent reacting and nonreacting flows, offering very long pulse sequences at high pulse energy and high repetition rate.

This work was funded by the Air Force Research Laboratory (FA8650-12-C-2200) and the Air Force Office of Scientific Research (Dr. Chiping Li, Program Manager). The authors acknowledge significant technical contributions from Drs. R. Feeler and J. Doster of Northrop Grumman Cutting Edge Optronics.

References

1. B. Böhm, C. Heeger, R. L. Gordon, and A. Dreizler, Flow Turbul. Combust. **86**, 313 (2010).
2. I. Boxx, C. D. Carter, M. Stöhr, and W. Meier, Exp. Fluids **54**, 1532 (2013).
3. "HD Series Product Datasheet," Edgewave GbmH, http://www.edge-wave.de/web/downloads/datenblatter/.
4. B. Thurow, N. Jiang, and W. R. Lempert, Meas. Sci. Technol. **24**, 012002 (2013).
5. J. Körner, J. Hein, H. Leibetrau, R. Seifert, D. Klöpfel, M. Kahle, M. Loeser, M. Siebold, U. Schramm, and M. C. Kaluza, Opt. Express **21**, 29006 (2013).
6. P. Wu and R. B. Miles, Opt. Lett. **25**, 1639 (2000).
7. P. Wu, W. R. Lempert, and R. B. Miles, AIAA J. **38**, 672 (2000).
8. A. Bräuer, S. R. Engel, S. Dowy, S. Luther, J. Goldlücke, and A. Leipertz, Opt. Express **18**, 24579 (2010).
9. J. D. Miller, M. N. Slipchenko, T. R. Meyer, N. Jiang, W. R. Lempert, and J. R. Gord, Opt. Lett. **34**, 1309 (2009).
10. M. N. Slipchenko, J. D. Miller, S. Roy, J. R. Gord, S. A. Danczyk, and T. R. Meyer, Opt. Lett. **37**, 1346 (2012).
11. M. N. Slipchenko, J. D. Miller, S. Roy, J. R. Gord, and T. R. Meyer, Opt. Express **21**, 681 (2013).
12. M. J. Papageorge, T. A. McManus, F. Fuest, and J. A. Sutton, Appl. Phys. B **115**, 197 (2014).
13. J. B. Michael, P. Venkateswaran, J. D. Miller, M. N. Slipchenko, J. R. Gord, S. Roy, and T. R. Meyer, Opt. Lett. **39**, 739 (2014).
14. W. Koechner, *Solid-State Laser Engineering*, 6th ed. (Springer Science, 2006).
15. R. Feeler, Cutting Edge Optronics, 20 Point West Boulevard, St. Charles, Missouri 63301 (personal communication, 2014).
16. "Rigel i1600 Product Datasheet," Powerlase Ltd, http://www.powerlase-photonics.com/products/1064nm/rigel-i1600/.
17. D. R. Dudley, O. Mehl, G. Y. Wang, E. S. Allee, H. Y. Pang, and N. Hodgson, Proc. SPIE **7193**, 71930Z (2009).